Impact of induced bandgaps on sub-Poissonian shot noise in graphene armchair-edge nanoribbons

G. J. Xu,[1] Y. M. Zhu,[1,a)] B. H. Wu,[2] X. G. Xu,[3,b)] and J. C. Cao[3,a)]
[1]*Engineering Research Center of Optical Instrument and System, Ministry of Education, Shanghai Key Lab of Modern Optical System, University of Shanghai for Science and Technology, 516 Jungong Road, Shanghai 200093, People's Republic of China*
[2]*Department of Applied Physics, Donghua University, 2999 North Renmin Road, Shanghai 201620, People's Republic of China*
[3]*Key Laboratory of Terahertz Solid-State Technology, Shanghai Institute of Microsystem and Information Technology, Chinese Academy of Sciences, 865 Changning Road, Shanghai 200050, People's Republic of China*

(Received 14 July 2012; accepted 12 September 2012; published online 10 October 2012)

The impact of the bandgap induced by transversal constriction on the sub-Poissonian properties of graphene armchair-edge nanoribbons (GANRs) has been investigated in a theoretical perspective. For a typical GANR with a bandgap, the minimal conductivity at the Dirac point becomes more suppressed than that of the gapless case $4e^2/\pi h$, and the Fano factor becomes more enhanced than the originally predicted value 1/3. The amplitudes of conductivity suppression and Fano factor enhancement will grow large as the nanoribbon width decreases. And the variance of Fano factor is qualitatively consistent with the reported experimental data. The carriers of GANRs with gaps behave like counterparticles in a semiconductor, and the transition from the sub-Poissonian to a Poissonian process takes place gradually with the reduction of the nanoribbon width. For the low aspect ratio (the sample width over its length) limit, the shot noise property at the Dirac point is no longer sensitive to the boundary edges. For the high limit, it requires a larger aspect ratio for the minimal conductivity and maximal Fano factor to achieve stationary values than that of the gapless case. © *2012 American Institute of Physics*. [http://dx.doi.org/10.1063/1.4758302]

I. INTRODUCTION

Graphene-based devices have developed rapidly since the experimental isolation of graphene.[1–7] Digital logic devices are of great potential in sorts of application perspectives.[4–7] The zero-bandgap dispersion of graphene leads to a minimal conductivity,[2] even for zero carrier density, which produces an extremely low on-off ratio, a fatal disadvantage in logic devices. To improve the performances, a few ways are developed to open bandgaps in the linear dispersion, such as tailing graphene into nanoribbons or quantum dots, biasing bilayer graphene, and applying strain to graphene.[7] In fact, graphene nanoribbon (GNR) is an ideal candidate to engineer band structures using conventional semiconductor technologies. The bandgap of GNRs is inversely linear with the nanoribbon width. The transport properties of this mesoscopic system have attracted enormous attention to unveil the mechanism of Dirac fermions.[8,9]

Shot noise originates from the discrete nature of electric charge. It may be dominant when the number of carriers is sufficiently small so that the current fluctuation in time due to the random distribution is of significance.[10] And it can be a source of information which is not contained in the time-averaged value, such as the Fano factor $F = 2$ denoting the Cooper pair in superconductors,[11] $F = 1/3$ implicating the filling fraction of the lowest Landau level in the fractional quantum Hall effect,[12] $F = 1/3$ also indicating the strongly conducting transmission channels in disordered gold wire,[13] and so on. The classical dynamics in the graphene strip should be a ballistic process at low temperature in the absence of impurity scattering, strain or other defects, and spin-orbit interaction. One can expect a Poisson process in such a graphene. However, Tworzydlo *et al.*[14] predicted in theory that the Fano factor of graphene strips at Dirac point equals 1/3, 3 times smaller than a Poisson process. It is the same value as for a disordered metal, which can be called sub-Poissonian shot noise. This extraordinary phenomenon has attracted much interest in theoretical[15–18] and experimental perspectives.[19,20] Sonin has analyzed the shot noise in the ballistic regime, which includes the comparison between the coherent and incoherent limit for arbitrary drops between leads and the central region[16] and the effect of Klein tunneling on the coherent transport properties.[18] Castro Neto's group has discussed the shot noise in disordered systems, including the dependence of conductance on the carrier density controlled by disorder strength and aspect ratio[15] and the edge roughness in graphene nanowires, which results in conductance suppression due to Anderson localization.[17] Simultaneously, this peculiar sub-Poissonian shot noise has been verified in experiment.[19,20] DiCarlo *et al.*[19] demonstrated that the Fano factor keeps steady within ±10% upon different carrier type and density and averages between 0.35 and 0.38. Here, we noted that the measured Fano factor is a little higher than the predicted value 1/3. And the quantum constriction along the transversal dimension can produce a

[a)]Electronic mail: ymzhu@usst.edu.cn; jccao@mail.sim.ac.cn.
[b)]Current address: State Key Laboratory of Functional Materials for Informatics, Shanghai Institute of Microsystem and Information Technology, Chinese Academy of Sciences, 865 Changning Road, Shanghai 200050, China.

nontrivial bandgap, which makes the dispersion deviate from the originally linear relationship. Maybe, the induced gap can explain the higher Fano factor observed in experiment.

It is the purpose of the present paper to investigate the influence of the induced gap on the sub-Poissonian shot noise in graphene armchair-edge nanoribbons (GANRs). The lateral quantum confinement makes the transversal wavevector discrete, producing an energy gap, which scales inversely with the nanoribbon width.[21,22] Moreover, the subband formation of GNRs is observed in experiments,[23] and a structured external potential can induce a spectral gap and realize the switch from metallic to insulating behavior.[24] Thus, it is possible to engineer the band gap by manipulating the width of GNR. The longitudinal and transversal momenta are not coupled by boundary edge in armchair-edge nanoribbons, while the zigzag edge is the very case where the longitudinal momentum couples with the transversal one, which will complicate the analytical solution. So we considered the graphene armchair-edge nanoribbons case for simplicity. Based on the previous works,[14,25] taking the induced bandgap into account, we have studied the changes of sub-Poissonian shot noise. The rest of the paper is organized as follows. In Sec. II, the model and formalism is described by using Dirac-fermion approach. In Sec. III, the transmission and conductivity of multi-modes are analyzed, and the effect of induced bandgap on the sub-Poissonian shot noise is discussed in details. A brief summary is concluded in Sec. IV.

II. MODEL AND FORMALISM

The model we considered is shown in Fig. 1. The aspect ratio (W/L) is of significance for GNRs, and the potential profile can be controlled via gate voltage.[26–28] Here, the microscopic mechanisms, such as the electron-phonon, electron-electron, and spin-orbit interaction, are assumed to be ignored, and the zero-temperature approximation is set in order to compare numerical results with others' experimental data. In the low energy regime ($\epsilon < 1\,\mathrm{eV}$) near Dirac points K and K', the wave functions can be described in terms of envelope functions $[\psi_A(\mathbf{r})], \psi_B(\mathbf{r})]^T$ and $[\psi'_A(\mathbf{r})], \psi'_B(\mathbf{r})]^T$, where A and B stand for the two interpenetrating triangle sublattices, respectively, and T stands for transposed matrix.[29] Thus, the complete wave function can be expressed as $\Psi(\mathbf{r}) = [\psi_A(\mathbf{r})], \psi_B(\mathbf{r}), \psi'_A(\mathbf{r})], \psi'_B(\mathbf{r})]^T$.

A. Dispersion and boundary

Taking the bandgap 2Δ induced by quantum restriction into account, the Dirac equation $[v_F(\sigma \cdot p) + U(x)]\Psi = E\Psi$ can be rewritten as

$$\begin{pmatrix} -i\hbar v_F(\sigma_x\partial x + \sigma_y\partial y) + \sigma_z\Delta & 0 \\ 0 & -i\hbar v_F(\sigma_x\partial x - \sigma_y\partial y) - \sigma_z\Delta \end{pmatrix}\Psi(\mathbf{r}) + U(x)\Psi(\mathbf{r}) = E\Psi(\mathbf{r}), \tag{1}$$

where

$$\Delta = hv_F/3W, \tag{2}$$

h is the Plank constant, $v_F \approx 10^8\,\mathrm{cm\cdot s^{-1}}$ is the Fermi velocity, σ_α is Pauli matrix ($\alpha = x, y, z$), and $U(x)$ is the potential profile. Eq. (2) is only a rough expression, and the bandgap is proved to be reversely linear with the width of GNRs, where the precise coefficient is distributed in a range.[21,22] The wavevectors can be denoted as k_x and k_y. For a fixed potential U, $\det|H - E| = 0$ can be expressed from Eq. (1) as

$$\begin{vmatrix} U + \Delta - E & \hbar v_F(k_x - ik_y) & 0 & 0 \\ \hbar v_F(k_x + ik_y) & U - \Delta - E & 0 & 0 \\ 0 & 0 & U - \Delta - E & \hbar v_F(k_x + ik_y) \\ 0 & 0 & \hbar v_F(k_x - ik_y) & U + \Delta - E \end{vmatrix} = 0. \tag{3}$$

Thus, the dispersion can be derived as

$$E = U \pm \sqrt{\Delta^2 + \hbar^2 v_F^2 k^2}, \tag{4}$$

where $k^2 = k_x^2 + k_y^2$. Eq. (4) is the disperse relation of GNRs with an energy gap. When the potential profile is $U = 0$, Fig. 2 presents the corresponding numerical results for various width of GNRs. With reducing the width, the induced bandgap 2Δ is becoming much more obvious in the vicinity of the Dirac point. In the low energy range, it deviates from its original linear relationship $E = \hbar v_F|k|$. Away from the Dirac point ($\hbar v_F|k| \gg \Delta$), it is recovering back to the approximately linear relation.

The wavevector k_y is discrete due to quantum transversal constriction in GNRs, and q_n can be substituted for k_y to distinguish from the longitudinal one k_x. The wave function for Eq. (1) can be written as

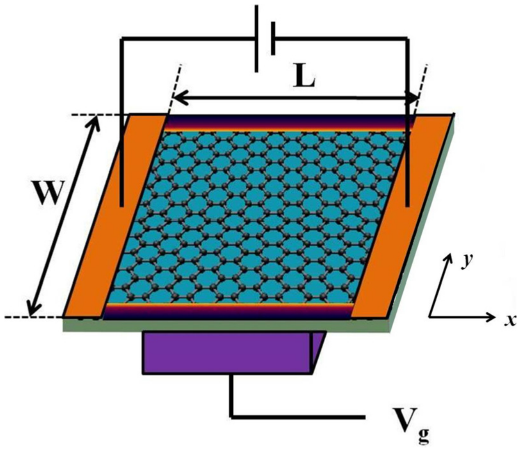

FIG. 1. Schematic diagram of a graphene strip, whose width and length are W and L, respectively. The gate voltage V_g is used to tune the carrier type and density in the strip.

$$\Psi_{n,k_x}(\mathbf{r}) = \chi_{n,k_x}(y)e^{ik_x x}, \tag{5}$$

where

$$\chi_{n,k_x}(y) = a_n \begin{pmatrix} 1 \\ z_{n,k_x}\gamma_{n,k_x} \\ 0 \\ 0 \end{pmatrix} e^{iq_n y} + a'_n \begin{pmatrix} 0 \\ 0 \\ z_{n,k_x}\gamma_{n,k_x} \\ 1 \end{pmatrix} e^{iq_n y} + b_n \begin{pmatrix} z_{n,k_x}\gamma_{n,k_x} \\ 1 \\ 0 \\ 0 \end{pmatrix} e^{-iq_n y} + b'_n \begin{pmatrix} 0 \\ 0 \\ 1 \\ z_{n,k_x}\gamma_{n,k_x} \end{pmatrix} e^{-iq_n y}, \tag{6}$$

where

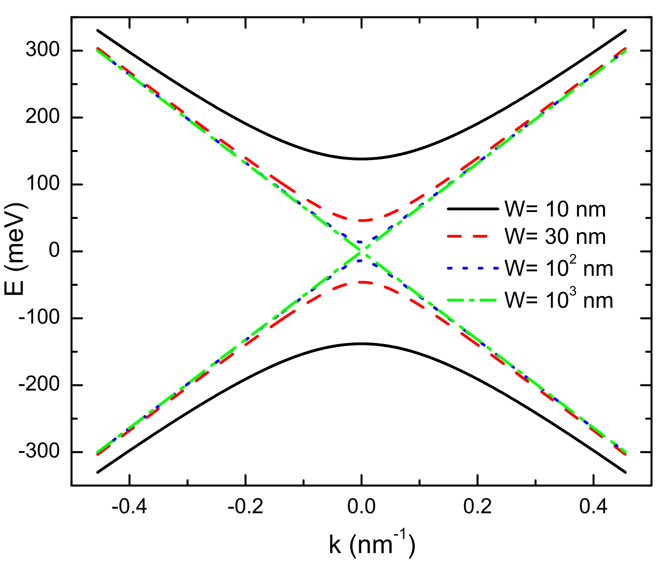

FIG. 2. Dispersion relations of various graphene strip widths $W = 10$ nm, $W = 30$ nm, $W = 10^2$ nm, and $W = 10^3$ nm, which are corresponding to the solid curve, dashed curve, dotted curve, and dotted-dashed curve, respectively. And the bandgap for the above GNRs are 276.2 meV, 92.07 meV, 27.62 meV, and 2.76 meV according to Eq. (2).

$$z_{n,k_x} = \lambda \frac{k_x + iq_n}{\sqrt{k_x^2 + q_n^2}}, \quad \gamma_{n,k_x} = \sqrt{\frac{\sqrt{\Delta^2 + \hbar^2 v_F^2 k^2} - \lambda\Delta}{\sqrt{\Delta^2 + \hbar^2 v_F^2 k^2} + \lambda\Delta}}, \tag{7}$$

with the sign function $\lambda = \mathrm{sgn}(E - U)$, $\lambda = +1$ for the conduction band and $\lambda = -1$ for the valence band. It is noticeable that $z_{n,k_x} z_{n,-k_x} = -1$, which will be used in later derivation. When $\Delta = 0$, the factor γ becomes $\gamma = 1$, back to the gapless case.

The transversal wavevector has been obtained for different boundary conditions from Ref. 14 as

$$q_n = (n + \alpha)\frac{\pi}{W}, \tag{8}$$

where $\alpha = 1/2$ for the infinite mass boundary condition (smooth edge), $\alpha = 0$ for the metallic armchair edge, and $\alpha = 1/3$ for semiconducting armchair case. The details of this procedure can be found in supplementary material of Ref. 14.

B. Conductivity and Fano factor

The potential profile $U(x)$ is assumed as

$$U(x) = \begin{cases} U_\infty, & x < 0 \text{ and } x > L \\ U_g, & 0 \le x \le L. \end{cases} \tag{9}$$

To identify the longitudinal wavevector in different regions, we denote it as k_x in terminals and $\tilde{k}_x$ in the central region. The transversal momentum q_n is associated with various boundary conditions from Eq. (8), and it is assumed to be the same in the whole system.

The transition between various states for incident electron with an energy E can be described by following wavefunctions as

$$\Psi = \begin{cases} \Phi_L = \chi_{n,k_x} e^{ik_x x} + r_n \chi_{n,-k_x} e^{-ik_x x}, & x < 0 \\ \tilde{\Phi} = \alpha_n \chi_{n,\tilde{k}_x} e^{i\tilde{k}_x x} + \beta_n \chi_{n,-\tilde{k}_x} e^{-i\tilde{k}_x x}, & 0 \le x \le L \\ \Phi_R = t_n \chi_{n,k_x} e^{ik_x(x-L)}, & x > L, \end{cases} \tag{10}$$

where r_n and t_n are reflection and transmission amplitude, respectively, and α_n and β_n can be obtained by the continuity of Ψ at $x = 0$ and $x = L$. The concrete process is as following:

$$\begin{pmatrix} 1 \\ z_{n,k_x}\gamma_{n,k_x} \end{pmatrix} + r_n \begin{pmatrix} 1 \\ z_{n,-k_x}\gamma_{n,-k_x} \end{pmatrix} = \alpha_n \begin{pmatrix} 1 \\ z_{n,\tilde{k}_x}\gamma_{n,\tilde{k}_x} \end{pmatrix} + \beta_n \begin{pmatrix} 1 \\ z_{n,-\tilde{k}_x}\gamma_{n,-\tilde{k}_x} \end{pmatrix}, \tag{11}$$

$$t_n \begin{pmatrix} 1 \\ z_{n,k_x}\gamma_{n,k_x} \end{pmatrix} = \alpha_n \begin{pmatrix} 1 \\ z_{n,\tilde{k}_x}\gamma_{n,\tilde{k}_x} \end{pmatrix} e^{i\tilde{k}_x L} + \beta_n \begin{pmatrix} 1 \\ z_{n,-\tilde{k}_x}\gamma_{n,-\tilde{k}_x} \end{pmatrix} e^{-i\tilde{k}_x L}. \tag{12}$$

Using $z_{n,k_x} z_{n,-k_x} = -1$ and $\gamma_{n,-k_x} = \gamma_{n,k_x}$, the transmission amplitude can be found as

$$t_n = \frac{\gamma_{k_x}\gamma_{\tilde{k}_x}(1+z_{k_x}^2)(1+z_{\tilde{k}_x}^2)}{(\gamma_{\tilde{k}_x}+\gamma_{k_x}z_{k_x}z_{\tilde{k}_x})(\gamma_{k_x}+\gamma_{\tilde{k}_x}z_{k_x}z_{\tilde{k}_x})e^{-i\tilde{k}_xL}+(\gamma_{k_x}z_{\tilde{k}_x}-\gamma_{\tilde{k}_x}z_{k_x})(\gamma_{\tilde{k}_x}z_{\tilde{k}_x}-\gamma_{k_x}z_{k_x})e^{i\tilde{k}_xL}}, \tag{13}$$

where the subindex n of z_{n,k_x} and γ_{n,k_x} in Eq. (13) are omitted for simplicity. Therefore, the transmission probability of the n mode can be expressed as $T_n = |t_n|^2$.

According to Landauer formula, one can find the conductance and the Fano factor of this system as

$$G = \frac{4e^2}{h}\sum_{n=0}^{N-1} T_n, \tag{14}$$

$$F = \frac{\sum_{n=0}^{N-1} T_n(1-T_n)}{\sum_{n=0}^{N-1} T_n}. \tag{15}$$

Based on Eq. (14), the conductivity is defined as $\sigma \equiv G \times L/W$.

III. NUMERICAL RESULTS AND DISCUSSIONS

The dispersion of various widths of GNRs is depicted in Fig. 2. With reducing the width, the induced bandgap becomes much more apparent. As for the aspect ratio, the length L is assumed to be varying correspondingly with the width W fixed, since the change of the width leads to the varying of the induced bandgap. About the gapless case, the zerogap is set as $\Delta = 0$, rather than calculated from Eq. (2) in this entire work, since every width corresponds to a bandgap. According to Eqs. (8) and (14), it is a multi-mode transport process for GANRs. To fulfill the calculation accuracy, the truncation of contributed modes is determined by $N = \mathrm{Int}(k_\infty W/\pi + 1/2)$, where $|U_\infty| = \hbar v_F k_\infty$. The potential in two terminals is assumed the same value $U_\infty = 1000\,\mathrm{meV}$, and the other parameters have already been illustrated in the following text. The impact of induced gaps on the multi-modes transport and sub-Poissonian shot noise will be discussed in details.

A. Multi-mode transport

The influence of the induced bandgap on a single-mode transmission probability for different boundary conditions is shown in Fig. 3. It is well-known that the transversal wave-vector q_n is linear with the mode-index n from Eq. (8). Thus, the energy threshold values for higher modes are increasing correspondingly, such as T_{10} and T_{20} in Fig. 3. When the bandgap is zero, the central region is completely transparent for zero-mode ($n=0$) transport of metallic armchair-edge boundary ($\alpha = 0$), as shown in Fig. 3(a), which corresponds

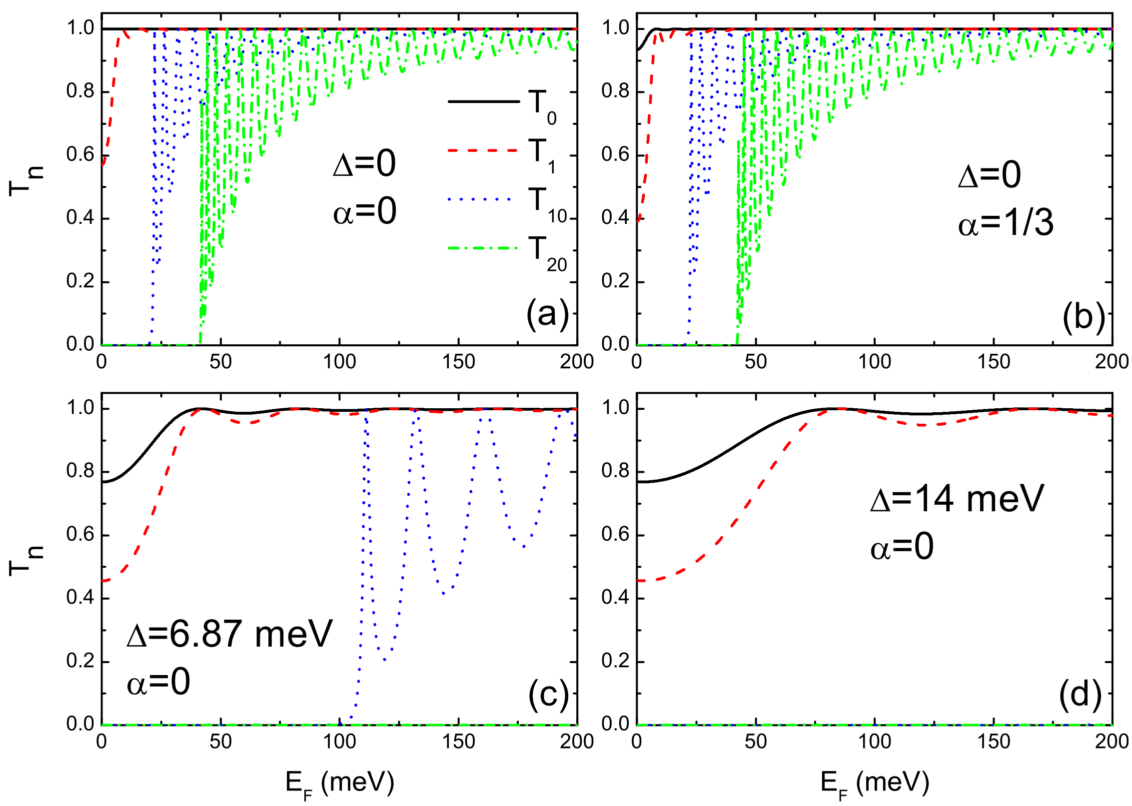

FIG. 3. The different modes transmission probability T_n versus incident energy E under various conditions (a) $\Delta = 0, \alpha = 0$, (b) $\Delta = 0, \alpha = 1/3$, (c) $\Delta = 6.87\,\mathrm{meV}, \alpha = 0$, and (d) $\Delta = 13.8\,\mathrm{meV}, \alpha = 0$. The potential of the two terminals is assumed to be $U_\infty = 1000\,\mathrm{meV}$, the gate voltage in the central region is $U_g = 0$, and the aspect ratio is $W/L = 4$. The widths of GNRs are the same 1000 nm in (a) and (b), and the widths are 200 nm and 100 nm in (c) and (d), respectively.

to the so-called "Klein tunneling"[30] due to the chirality conservation ($q_0 = 0$). For the semiconductor edge ($\alpha = 1/3$), there is no Klein tunneling emerging in Fig. 3(b) because of the minimal transversal momentum $q_0 = \pi/3W$. The induced bandgap has made Klein tunneling of the metallic-edge disappear, which can be seen in Figs. 3(c) and 3(d). Because the dispersion of GANRs has deviated from the original linear relationship, which can be seen from Fig. 2, therefore the carriers no longer obey the chirality conservation. The complete transmission is becoming an oscillatory phenomenon, which is related with the resonant tunneling as that in a semiconductor. In the low energy regime, the transmission probability of low-modes is reduced by the bandgap, and the emergences of high-modes are delayed due to the increased threshold values. Besides, the energy spaces between adjacent resonant levels are increasing as the width of GANRs decreases. Moreover, the oscillating period is also becoming evidently larger from Figs. 3(c) and 3(d), which is analogous to that in semiconductors. In other words, the bandgap makes the carriers in GANRs behave like those in semiconductors. As for semiconductor boundary ($\alpha = 1/3$) and smooth edge ($\alpha = 1/2$), the changes of transport properties by the bandgap are similar with that of the metallic case, except for the disappear of the Klein tunneling phenomenon of zero-mode. The bandgap makes the transmission of each mode in GANRs less sensitive than the gapless case.

According to Eq. (14), the summation over all modes leads to the conductivity of the system. The conductivity varying of the GANR with a metallic edge for different bandgaps is given in Fig. 4. As discussed above, the transmission probabilities of effective modes with contribution to conductivity have been reduced by induced bandgaps. And the energy thresholds of discrete modes increase with the bandgap. Thus, the conductivity of GANRs with a bandgap has been much suppressed, as shown by curves 1 and 2 in Fig. 4. And the tiny oscillation of the curves originates from the resonant tunneling of new opening channels, which can be seen from Fig. 3. When the bandgap grows larger further,

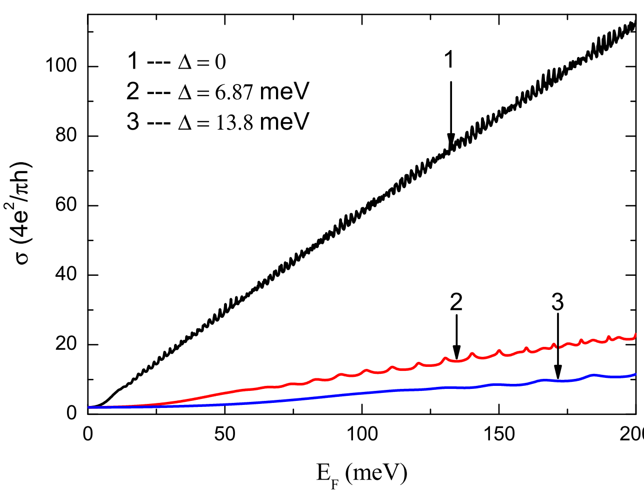

FIG. 4. The dependence of conductivity σ on incident energy E under various bandgap for the metallic edge. The curves marked 1, 2, and 3 correspond to different GNRs widths 1000 nm, 200 nm, and 100 nm. The other parameters are the same as that in Fig. 3.

the suppression of the conductivity is becoming more obvious, as seen from the curve 3. Moreover, the conductivity oscillates more smoothly, since the energy space between adjacent resonant levels becomes larger. The oscillation is almost invisible in curve 3 of Fig. 4. Compared with the gapless GANRs, the same feature is that the conductivity with a bandgap is roughly linear with the incident energy, owing to the linear dependence of the new-opening mode level E_n on index n.

B. Conductivity and Fano factor

When the Fermi level is at the Dirac point, the impact of the bandgaps on the conductivity and Fano factor of GANRs for smooth edge ($\alpha = 0.5$) and metallic boundary ($\alpha = 0$) is depicted in Fig. 5. When there is no induced gaps($\Delta = 0$), for the low aspect ratio limit $W/L \to 0$, the most exceptional part of the metallic edge is that the absence of the 1/2 offset in the transverse momentum q_n leads to the transition from insulating to metallic. Meanwhile, for the high limit $W/L \to \infty$, the edge has no effect on the conductivity ($\sigma \to g_0/\pi$) and Fano factor ($F \to 1/3$), as shown in Figs. 5(a) and 5(b), which is in excellent agreement with the results from Eq. (16) in Ref. 14

$$T_n = \frac{1}{\cosh^2 Lq_n + (q_n/k_\infty)^2 \sinh^2 Lq_n} \to \frac{1}{\cosh^2[\pi(n+\alpha)L/W]}. \tag{16}$$

The influence of induced bandgap on the conductivity and shot noise is clearly distinguished, even for a subtle gap ($2\Delta = 11.04\,\text{meV}$) as presented in Figs. 5(c) and 5(d). The most distinct change is that the properties of GANRs are independent on edge conditions. For the limit $W/L \to 0$, the conductivity and Fano factor of the metallic edge are reversed completely. The original gapless system of the metallic edge is analogous with a quantum point, with all channels open, and the Fano factor is zero as seen in Fig. 5(b). After considering the bandgap, it is similar with a tunneling junction, with low transmission channels, and the Fano factor becomes one as shown in Fig. 5(d). The induced bandgap makes the properties no longer sensitive to the boundary edge, as indicated from the almost coincident curves in Figs. 5(c) and 5(d). Moreover, for the high limit $W/L \to \infty$, it requires a larger aspect ratio than that of the gapless case for the conductivity and Fano factor to achieve stationary values. These phenomena are much more obvious with the reduction of GANRs width. Actually, it is similar with the shot noise in Figs. 5(c) and 5(d) for the semiconducting boundary edge $\alpha = 1/3$.

With a moderate aspect ratio fixed ($W/L = 5$), the minimal conductivity and the maximal Fano factor for different bandgaps at the Dirac point can be obtained by varying the gate voltage, as shown in Fig. 6. For the zero-bandgap case, the limiting characteristics of a short and wide strip ($W/L \to \infty$) agrees well with the formulas in Ref. 14

$$\sigma \to 4e^2/h\pi, \qquad F \to 1/3, \tag{17}$$

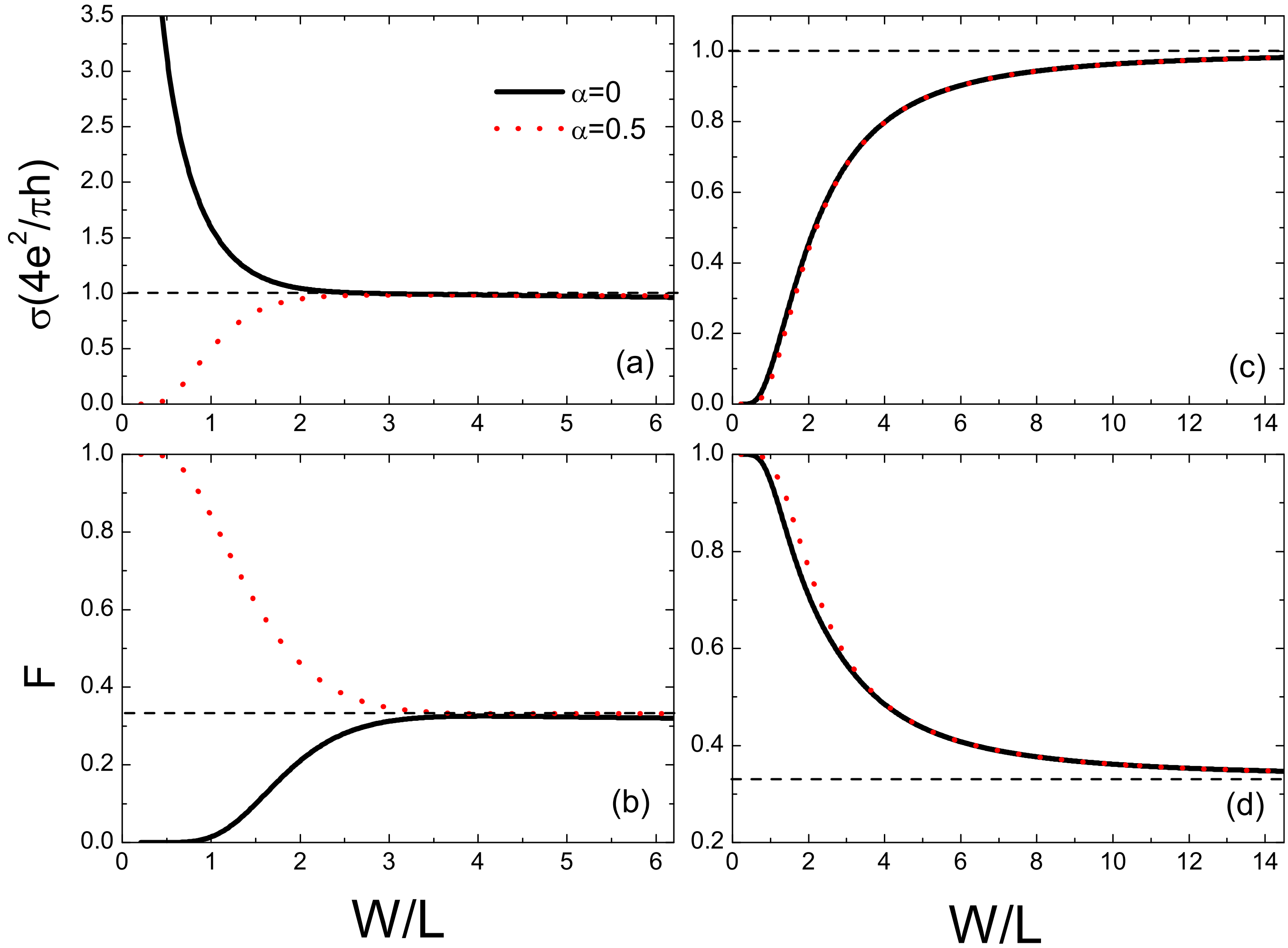

FIG. 5. The conductivity σ and Fano factor F versus aspect ratio W/L for different bandgap conditions ($\Delta = 0$ for (a) and (b), $\Delta \neq 0$ for (c) and (d)). The solid lines and the dotted lines are corresponding to the smooth edge and metallic edge, respectively. The dashed line $\sigma = 1$ in (a) and (c), $F = 1/3$ in (b) and (d) are for eye guidance. The width of GNR is 500 nm, and the other parameters are the same as that in Fig. 3.

as seen in Figs. 6(a) and 6(b). The behavior is associated with the well-known minimal conductivity, which originates from the evanescent transmission at the Dirac point in despite of the carrier types and density. And this phenomenon is universal for the most general boundary condition at various edges of the graphene strip. Taking the induced bandgap ($\Delta \neq 0$) into account, although the varying profile of conductivity and shot noise at the Dirac point are almost alike with those of the gapless case, the conductivity has shifted to a lower value ($\sigma \rightarrow 0.86 \times 4e^2/h\pi$) and the Fano factor has shifted to a higher value ($F \rightarrow 0.44$), as plotted in Figs. 6(c) and 6(d). Actually, these results can be also derived in Figs. 5(c) and 5(d) with the fixed aspect ratio ($W/L = 5$). The Fano factor values measured in experiment[19] distribute between 0.35 and 0.38, a little higher than the theoretical prediction.[14] The typical value 0.44 in our work is sort of higher than the experimental value range due to the width difference between their sample width $W = 2\,\mu$m and ours $W = 500$ nm. The induced gap in the experiment is $2\Delta = 2.76$ meV, much lower than ours $2\Delta = 11.04$ meV, then the impact of gaps on the shot noise is smaller than our calculation. Thus our conclusion is qualitatively consistent with the observed results in experiment. The emergence of the bandgap, even with a tiny amplitude, has reduced the minimal conductivity to a direction of "off" state and enhanced the sub-Poissonian transport to a Poisson process. It is easy to understand that the GANRs with an energy gap become the analogues of semiconductors. These changes are much more evident with reducing the GANR width. The oscillation of the conductivity and Fano factor in both high gate voltage sides indicates the jittering motion of confined Dirac fermions, which is called "Zitterbewegung," a consequence of the interference of states with positive and negative energy.[14] The influence of gaps on this property is relatively weak. The sub-Poissonian shot noise at the Dirac point is independent of various boundary edges regardless of the bandgap, as seen in Fig. 6.

The sub-Poissonian shot noise phenomenon in GANRs, where the Fano factor is 1/3, originates from the evanescent transmission of carriers at the charge-neutrality point (Dirac point).[14] The Fano factor value 1/3 also appears in disordered metals, which is a consequence of classical diffusive dynamics. Remarkably, the dynamical transport of an ideal graphene strip is a ballistic process, and one can expect a Poisson process with the corresponding Fano factor $F = 1$. The observed value in experiment is a little higher than the predicted 1/3.[19] In our work, we could explain the measured

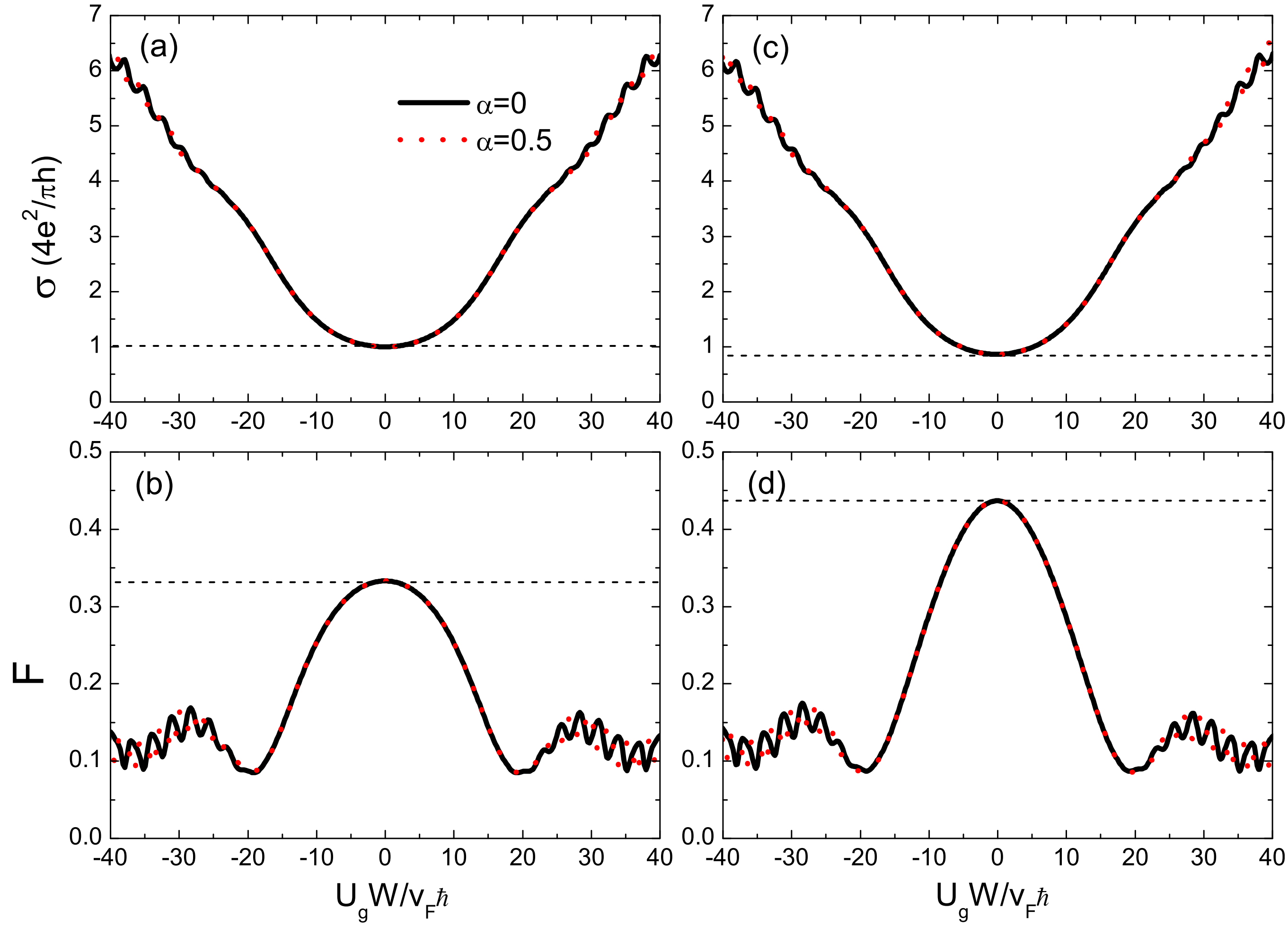

FIG. 6. Fermi energy dependence of the conductivity σ and Fano factor F with a fixed aspect ratio for different bandgap conditions ($\Delta = 0$ for (a) and (b), $\Delta \neq 0$ for (c) and (d)). The solid lines and the dotted lines are corresponding to the smooth edge and metallic edge, respectively. The dashed lines $\sigma = 4e^2/h\pi$ in (a), $F = 1/3$ in (b), $\sigma = 0.86 \times 4e^2/h\pi$ in (c), and $F = 0.44$ in (d) are for eye guidance. The width of GNR is 500 nm, the aspect ratio is $W/L = 5$, and the other parameters are the same as that in Fig. 3.

higher Fano factor via the induced bandgap. The variance of the shot noise can help us to extract the useful information for logic devices characterization.

IV. CONCLUSION

In this work, we have investigated the influence of the bandgap induced by transversal constriction on the sub-Poissonian shot noise properties of GANRs. The bandgap leads to the deviation from an ideally linear dispersion, and then the transmission is suppressed due to the broken of chirality conversation. Taking the bandgap into account, we found that the minimal conductivity at the Dirac point becomes more suppressed than that of the gapless case $4e^2/\pi h$, and the Fano factor becomes more enhanced than the originally predicted value 1/3. The amplitudes of conductivity suppression and Fano factor enhancement are going to become large when the width of GANRs decreases. The bandgap can be used to explain the higher Fano factor observed in experiment qualitatively as a correction. The GANRs with gaps are becoming analogues of semiconductors, and the transition from the sub-Poissonian to a Poissonian process is taking place gradually with reducing the nanoribbon width. About the geometry of GANRs, for the low aspect ratio limit, the bandgap makes the shot noise properties at the Dirac point no longer sensitive to the boundary edges. Especially, it has completely changed the features of metallic-edge GANRs oppositely. For the high limit, the aspect ratio required for the minimal conductivity and maximal Fano factor to achieve stationary values is increasing obviously. These results can help us to understand the sub-Poissonian shot noise and extract the useful transport information of devices.

ACKNOWLEDGMENTS

This work was supported by the 863 Program of China (Project No. 2011AA010205), the National Natural Science Foundation of China (Grant Nos. 61131006 and 11074266), the Major National Development Project of Scientific Instrument and Equipment (Grant No. 2011YQ150021), the Important National Science and Technology Specific Projects (Grant No. 2011ZX02707), the Major Project (Project No. YYYJ-1123-1) of the Chinese Academy of Sciences, and the Shanghai Municipal Commission of Science and Technology (Project No. 10JC1417000).

[1]K. S. Novoselov, A. K. Geim, S. V. Morozov, D. Jiang, Y. Zhang, S. V. Dubonos, I. V. Grigorieva, and A. A. Firsov, Science **306**, 666 (2004).
[2]K. S. Novoselov, A. K. Geim, S. V. Morozov, D. Jiang, M. I. Katsnelson, I. V. Grigorieva, S. V. Dubonos, and A. A. Firsov, Nature (London) **438**, 197 (2005).
[3]Y. Zhang, Y. W. Tan, H. L. Stormer, and P. Kim, Nature (London) **438**, 201 (2005).
[4]A. K. Geim, Science **324**, 1530 (2009).
[5]F. Bonaccorso, Z. Sun, T. Hasan, and A. C. Ferrari, Nat. Photonics **4**, 611 (2010).
[6]P. Avouris, Nano Lett. **10**, 4285 (2010).
[7]F. Schwierz, Nat. Nanotechnol. **5**, 487 (2010).
[8]A. H. C. Neto, F. Guinea, N. M. R. Peres, K. S. Novoselov, and A. K. Geim, Rev. Mod. Phys. **81**, 109 (2009).
[9]S. D. Sarma, S. Adam, E. H. Hwang, and E. Rossi, Rev. Mod. Phys. **83**, 407 (2011).
[10]Ya. M. Blanter and M. Büttiker, Phys. Rep. **336**, 1 (2000).
[11]F. Lefloch, C. Hoffmann, M. Sanquer, and D. Quirion, Phys. Rev. Lett. **90**, 067002 (2003).
[12]C. L. Kane and M. P. A. Fisher, Phys. Rev. Lett. **72**, 724 (1994).
[13]A. H. Steinbach, J. M. Martinis, and M. H. Devoret, Phys. Rev. Lett. **76**, 3806 (1996).
[14]J. Tworzydlo, B. Trauzettel, M. Titov, A. Rycerz, and C. W. J. Beenakker, Phys. Rev. Lett. **96**, 246802 (2006).
[15]C. H. Lewenkopf, E. R. Mucciolo, and A. H. C. Neto, Phys. Rev. B **77**, 081410(R) (2008).
[16]E. B. Sonin, Phys. Rev. B **77**, 233408 (2008).
[17]E. R. Mucciolo, A. H. C. Neto, and C. H. Lewenkopf, Phys. Rev. B **79**, 075407 (2009).
[18]E. B. Sonin, Phys. Rev. B **79**, 195438 (2009).
[19]L. DiCarlo, J. R. Williams, Y. Zhang, D. T. McClure, and C. M. Marcus, Phys. Rev. Lett. **100**, 156801 (2008).
[20]R. Danneau, F. Wu, M. F. Craciun, S. Russo, M. Y. Tomi, J. Salmilehto, A. F. Morpurgo, and P. J. Hakonen, Phys. Rev. Lett. **100**, 196802 (2008).
[21]Y.-W. Son, M. L. Cohen, and S. G. Louie, Phys. Rev. Lett. **97**, 216803 (2006).
[22]M. Y. Han, B. Özyilmaz, Y. Zhang, and P. Kim, Phys. Rev. Lett. **98**, 206805 (2007).
[23]Y.-M. Lin, V. Perebeinos, Z. Chen, and P. Avouris, Phys. Rev. B **78**, 161409(R) (2008).
[24]W. Apel, G. Pal, and L. Schweitzer, Phys. Rev. B **83**, 125431 (2011).
[25]M. R. Setare and D. Jahani, Physica B **405**, 1433 (2010).
[26]H. B. Heersche, P. Jarillo-Herrero, J. B. Oostinga, L. M. K. Vandersypen, and A. F. Morpurgo, Nature (London) **446**, 56 (2007).
[27]F. Miao, S. Wijeratne, Y. Zhang, U. C. Coskun, W. Bao, and C. N. Lau, Science **317**, 1530 (2007).
[28]J. R. Willams, L. DiCarlo, and C. M. Marcus, Science **317**, 638 (2007).
[29]L. Brey and H. A. Fertig, Phys. Rev. B **73**, 235411 (2006).
[30]M. I. Katsnelson, K. S. Novoselov, and A. K. Geim, Nat. Phys. **2**, 620 (2006).